JPE 18-1-22

https://doi.org/10.6113/JPE.2018.18.1.234
ISSN(Print): 1598-2092 / ISSN(Online): 2093-4718

Line Impedance Estimation Based Adaptive Droop Control Method for Parallel Inverters

Phuong Minh Le[*], Xuan Hoa Thi Pham[**], Huy Minh Nguyen[*], Duc Duy Vo Hoang[*], Tuyen Dinh Nguyen[*], and Dieu Ngoc Vo[†]

[*]Dept. of Power Delivery, Hochiminh City University of Technology, VNU-HCM, Ho Chi Minh City, Vietnam
[**]Dept. of Electrical and Electronic Engineering, University of Food Industry, Ho Chi Minh City, Vietnam
[†]Dept. of Power Systems, Hochiminh City University of Technology, VNU-HCM, Ho Chi Minh City, Vietnam

Abstract

This paper presents a new load sharing control for use between paralleled three-phase inverters in an islanded microgrid based on the online line impedance estimation by the use of a Kalman filter. In this study, the mismatch of power sharing when the line impedance changes due to temperature, frequency, significant differences in line parameters and the requirements of the Plug-and-Play mode for inverters connected to a microgrid has been solved. In addition, this paper also presents a new droop control method working with the line impedance that is different from the traditional droop algorithm when the line impedance is assumed to be pure resistance or pure inductance. In this paper, the line impedance estimation for parallel inverters uses the minimum square method combined with a Kalman filter. In addition, the secondary control loops are designed to restore the voltage amplitude and frequency of a microgrid by using a combined nominal value SOGI-PLL with a generalized integral block and phase lock loop to monitor the exact voltage magnitude and frequency phase at the PCC. A control model has been simulated in Matlab/Simulink with three voltage source inverters connected in parallel for different ratios of power sharing. The simulation results demonstrate the accuracy of the proposed control method.

Key words: Droop control, Impedance estimation, Kalman filter, Microgrid

I. INTRODUCTION

With the expansion of the electrical power grid, conventional power systems have become increasingly vulnerable when it comes to coping with the reliability requirements and the diverse demand of power users. Moreover, distributed generation (DG) has advantages such as pollution reduction, high-energy utilization rate, flexible installation location, and low-power transmission losses [1], [2]. DG units also have a higher degree of controllability and operability when compared to conventional generators, which allows microgrids to play a major and critical role in maintaining the reliability and stability of electric networks [3]-[6]. Therefore, microgrids will gradually become a strong and effective support for the main power grid and a potential trend for future power systems [7].

In fact, the renewable energy resources such as wind, solar and tidal energy are connected to conventional grids through converters and microgrids are formed before they are connected to grids [8]-[12]. In the grid-connected mode, the DG units are often controlled as follows. The most widely adopted control strategies for grid-following inverters are discussed in [4], [7], [13], [14]. When a microgrid is operating in the islanded mode, each of the DG units should be able to supply its share of the total load in proportion to its rating. The control strategies for this mode are usually divided into two main types [11], [15] as follows. The first type is made up of the communication-based control techniques including concentrated control, master/slave control and distributed control. These techniques can achieve an excellent voltage regulation and proper power sharing. However, these control strategies required communication lines between the modules which may increase cost of systems. Long distance communication lines are easier to disrupt, which reduces system reliability and expandability. The second type is based on the droop control technique without requiring communications, and it is widely used in conventional power

Manuscript received Oct. 11, 2016; accepted Sep. 27, 2017
Recommended for publication by Associate Editor Jae-Do Park.
[†]Corresponding Author: vndieu@gmail.com
Tel: +(84.28) 38647257–Ext. 5730, Fax: +(84.28) 38 645 796, HCMUT
[*]Dept. of Power Del., Hochiminh City Univ. Tech., VNU-HCM, Vietnam
[**]Dept. of Electrical and Electron. Eng., Univ. of Food Ind., Vietnam

systems [2], [3], [8], [16]-[22]. The reason for the popularity of this droop control technique is that it provides a decentralized control capability that does not depend on external communication links. These techniques enable the "plug-and-play" interface and enhance the reliability of systems. However, communications can be used in addition to the droop control method to enhance the system performance without reducing reliability [23]-[30].

Traditional droop control techniques have some disadvantages such as a slow response to changes in the load, inaccuracy in power sharing, unbalanced harmonic current and dependent on the line impedance of inverters [11]. In addition, there are difficulties in the power sharing due to the following reasons:

- The line impedances are not available and different from each other. This has a significant effect on power sharing due to different voltage drops. When the impedances of the lines connecting inverters to the common connection point are different, a current imbalance appears when the load sharing error increases [1].
- The heterogeneous line impedance, including the resistor and capacitance, is not suitable for conventional droop control with pure resistors or pure capacitance applying for the low voltage distribution [1], [22]. Moreover, with a heterogeneous line impedance, the active and reactive power interact with each other, which leads to difficulty for separate control [1].
- Since line impedance changes due to temperature, the installation position no longer makes the system response more accurate.

Although frequency droop techniques can achieve accurate real power sharing, they typically result in poor reactive power sharing due to mismatches in the impedances of the DG unit feeders and the different ratings of the DG units [22]-[24]. Consequently, the problem of reactive power sharing in islanded microgrids has received considerable attention in the literature and many control techniques have been developed to address this issue [31], [32]. A comprehensive treatment of the concept of virtual impedance to mitigate errors in reactive power sharing is presented in [23]-[30]. This treatment has focused on the mismatch at the output impedances of the closed-loop controlled inverters that are used to interface with DG units. With a proper design of the voltage controller, the closed-loop output impedances are negligible at the steady state at around the nominal operating frequency. Therefore, the virtual impedance can result in accurate reactive power sharing. However, the analysis in [23]-[30] did not consider mismatches in the physical impedance of the feeders, including the transformers, cables and interface inductors associated with each DG unit.

An interesting droop control strategy has been proposed in [21]. The control strategy is composed of two stages including an initial conventional droop-based control stage and a synchronized compensation stage. The frequency droop is used to control reactive power sharing and an integral control term is added to the voltage droop to maintain the accuracy of the real power sharing. However, load changes during the compensation period or between the compensation periods may result in a poor power sharing. On the other hand, the control strategy introduced in [33] requires that the feeder impedances be resistive. The obtained results from the control strategy reflect accurate power sharing if this condition is satisfied. However, in practice, the feeders may have both ineligible inductive and resistive components. Therefore, each DG unit should be able to supply the same rating as analyzed in [34]. If they have different ratings, the strategy will not work. Therefore, the communication network is used as in [35], [36] to facilitate the estimation of the feeder impedances, which are then used to set the virtual impedances to ensure accurate reactive power sharing. The feeder impedance is estimated at the local DG controller by utilizing the point of common coupling (PCC), where the voltage harmonic data is transferred via a communication link. This is based on the assumption that the phase angle difference between the voltages at the PCC and the inverter output is negligible. This assumption may not hold for long feeders or for higher power levels.

This paper proposes a new method for droop control allowing an accurate load sharing ratio between the parallel inverters in islanded microgrids with the line impedance estimated online in terms of the conventional resistor. Moreover, the line impedance may vary depending on the temperature or frequency at the same time as significant differences between the inverters. The estimation blocks provide the line impedance parameters in real time for the proposed droop controller, which was built based on the minimum squares algorithm combined with a Kalman filter. In addition, secondary control loops are designed to restore the voltage amplitude and frequency of the microgrid by using a combined nominal value SOGI-PLL with a generalized integral block and phase lock loop to monitor the exact voltage magnitude and frequency phase at the PCC. Therefore, the proposed adaptive droop control method can be an alternative for load sharing control in islanded microgrids.

II. ISLANDED MICROGRID STRUCTURE

The structure of an islanded microgrid composes of many inverters connected in parallel. In Fig. 1, a block diagram of two inverters is provided. Each inverter is connected to a common bus at the PCC through the line impedance. In addition, the loads of the microgrd are also connected to the common bus. The droop controller contains two control loops, where the outer loop power control divides the capacity of each inverter and the inner loop control makes the voltage and current output of the inverters similar to the references. The parameter estimation block provides the line impedance parameters in real time. Voltage and current signals from the

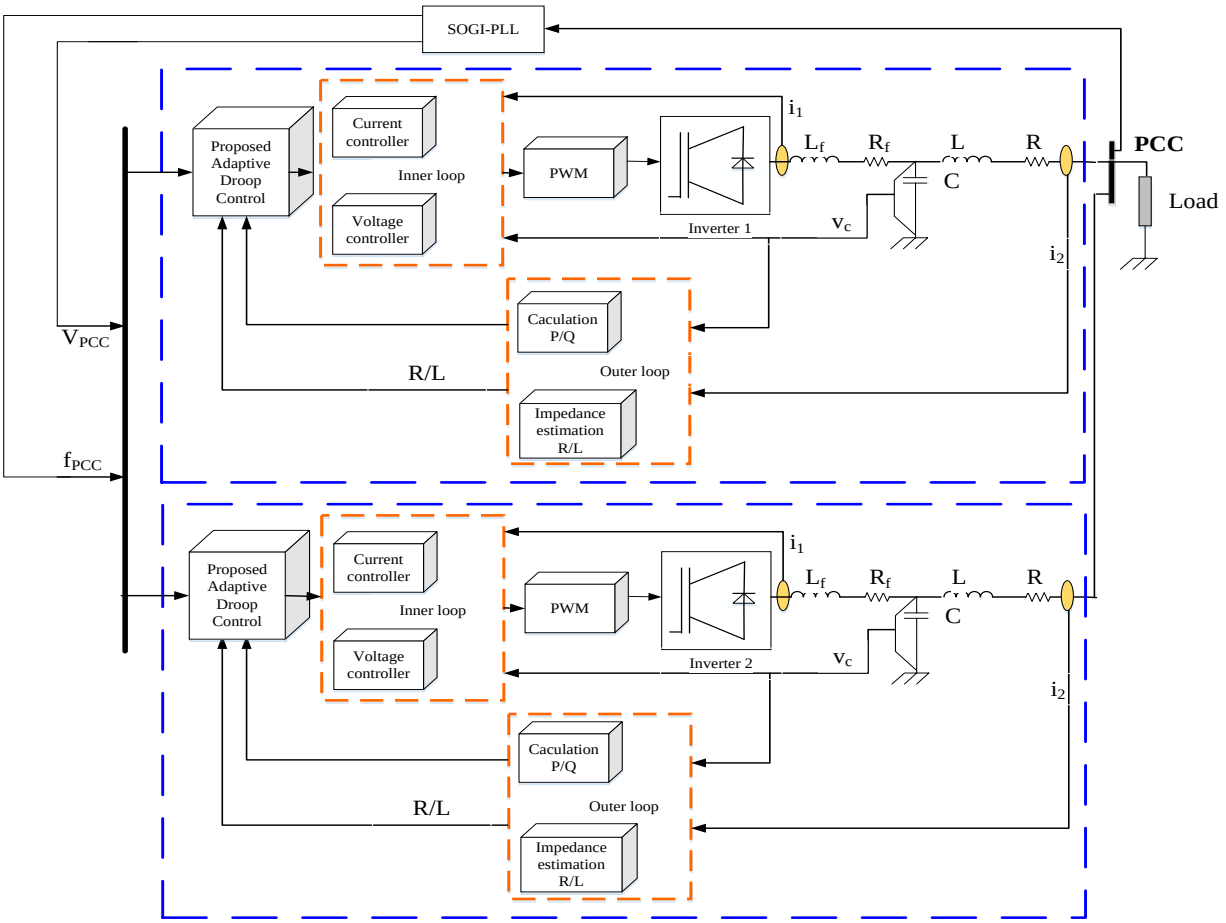

Fig. 1. Block diagram of an islanded microgrid.

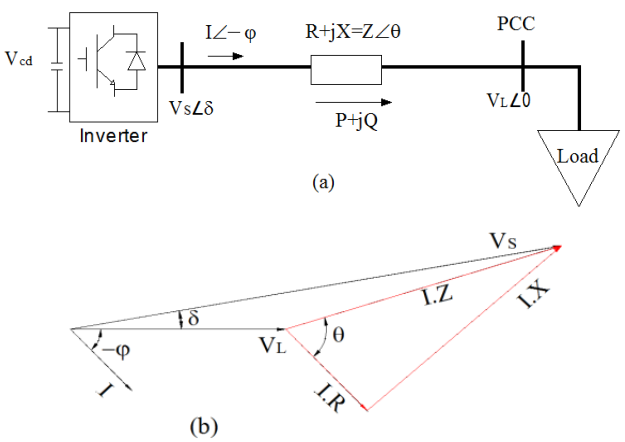

Fig. 2. (a) Equivalent schematic of inverters connected to a load; (b) vector diagram of voltage and current.

PCC are provided by a low-bandwidth connection. The inner loops are the current and voltage control to adjust the current and voltage at the inverter output. The SOGI-PLL (Second Order Generalized Integrator - Phase Locked Loop) block determines the amplitude and phase angle of the voltage at the PCC and supports the information for the adaptive controller droop.

III. ISLANDED MICROGRID CONTROL

A. The Proposed Droop Control

The principle of the droop control method is explained by considering the equivalent circuit of an inverter connected to an AC bus. The analysis method is based on Thevenin theorem as shown in Fig. 2. The active and reactive power supplied by the inverter are calculated as follows:

$$P = \frac{V_S}{R^2 + X^2}[R(V_S - V_L cos\delta) + XV_L sin\delta] \quad (1)$$

$$Q = \frac{V_S}{R^2 + X^2}[-RV_L sin\delta + X(V_S - V_L cos\delta)] \quad (2)$$

In general, both the inductance X and resistor R are considered. The use of an orthogonal linear rotational transformation matrix T from active power P and reactive power Q to active power P' and reactive power Q' is determined by:

$$\begin{bmatrix} P' \\ Q' \end{bmatrix} = [T]\begin{bmatrix} P \\ Q \end{bmatrix} = \begin{bmatrix} \frac{R}{Z}P + \frac{X}{Z}Q \\ -\frac{X}{Z}P + \frac{R}{Z}Q \end{bmatrix}\begin{bmatrix} P \\ Q \end{bmatrix} \quad (3)$$

When the power angle δ is small, equations (1), (2) and (3) can be rewritten as:

$$\delta \cong -\frac{ZQ'}{V_S V_L}\ ; V_S - V_L \cong \frac{ZP'}{V_S} \tag{4}$$

From (4), the basis of the well-known frequency and voltage droop regulation through active and reactive power is calculated by:

$$\omega = \omega_0 + m_q Q' \tag{5}$$

$$V_S = V_0 - m_p P' \tag{6}$$

where V_0 and ω_0 are the nominal amplitude voltage and frequency of the inverter, respectively; V_S and ω are the measured amplitude voltage and frequency of the inverter, respectively; and m_p and m_q are the active and reactive droop coefficients, which are calculated as follows:

$$m_q = \frac{\omega_{max} - \omega_{min}}{Q_{max}}\ ; m_p = \frac{V_{max} - V_{min}}{P_{max}} \tag{7}$$

The impedance of the lines connecting the inverters to the PCC is significantly different, the load sharing accuracy is difficult to achieve and voltage adjustment is difficult because it depends on the parameters of the system. From (5) and (6), the following are obtained:

$$m_{q1}Q_1' = m_{q2}Q_2' = \cdots = m_{qn}Q_n' = \Delta\omega_{max} \tag{8}$$

$$m_{p1}P_1' = m_{p2}P_2' = \cdots = m_{pn}P_n' = \Delta V_{max} \tag{9}$$

Combining the equations (1), (2), (3), (5), (6), (8) and (9), produces the conditions for accurately rated power sharing as in (10):

$$\begin{cases} \dfrac{m_{q1}}{Z_1} = \dfrac{m_{q2}}{Z_2} \\ \delta_1 = \delta_2 \\ V_{S1} = V_{S2} \\ \dfrac{m_{p1}}{Z_1} = \dfrac{m_{p2}}{Z_2} \end{cases} \tag{10}$$

To satisfy (10), it is necessary to choose droop coefficients that are proportional to the line impedance. If the system is adjusted to meet the requirements, the droop affects the quality of the frequency and voltage. Therefore, an adaptive controller droop is proposed to ensure the accurate power sharing of parallel inverters.

1) The Proposed Real Power Sharing Controller

The proposed droop controller uses equation (6). Then the voltage of the inverter is calculated as:

$$\mathrm{V_{S1}} = \mathrm{k_{p1}} \int \left(\mathrm{V_{S1\_ref}} - \mathrm{V_{PCC}}\right) \mathrm{dt} \tag{11}$$

$$\mathrm{V_{S1\_ref}} = \mathrm{V_{01}} - \mathrm{m_{p1}P_1'} \tag{12}$$

where k_{p1} is the gain of the integral, and V_{pcc} is the voltage at the PCC.

From (1), (2) and (3), it is possible to write:

$$P_1' = \frac{V_{S1}^2 - V_{S1}V_{PCC}\cos(\delta_1 - \delta_{PCC})}{Z_1} \tag{13}$$

$$Q_1' = -\frac{V_{S1}V_{PCC}\sin(\delta_1 - \delta_{PCC})}{Z_1} \tag{14}$$

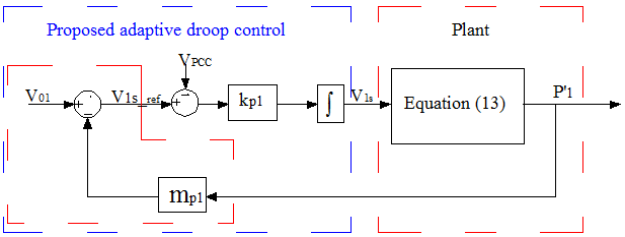

Fig. 3. Proposed adaptive real power sharing droop control.

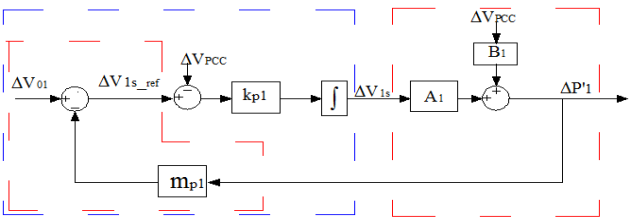

Fig. 4. Small signal adaptive real power sharing droop control.

where R_1 and X_1 are the outputs from the line impedance estimation, V_{pcc} and δ_{pcc} are the outputs of the SOGI-PLL blocks, V_{1s} is the output of the real power sharing from the controller, and δ_1 is the output of the reactive power sharing controller.

The relationships among (11), (12) and (13) are shown in Fig. 3.

By linearizing (11), (12) and (13) around P_1', V_1, V_{pcc}, δ_1 and δ_{pcc} the following is obtained:

$$\Delta V_{S1} = k_{p1} \int \left(\Delta V_{S1\_ref} - \Delta V_{PCC}\right) dt \tag{15}$$

$$\Delta V_{S1\_ref} = \Delta V_{01} - m_{p1}\Delta P_1' \tag{16}$$

$$\Delta P_1' = A_1 \Delta V_{S1} + B_1 \Delta V_{PCC} \tag{17}$$

where:

$$A_1 = \frac{2V_{S1} - V_{PCC}\cos(\delta_1 - \delta_{PCC})}{Z_1}$$

$$B_1 = -\frac{V_{S1}}{Z_1}\cos(\delta_1 - \delta_{PCC})$$

The relationships among (15), (16) and (17) are shown in Fig. 4.

The transfer function of Figure 4 is as follows:

$$\Delta P_1'(S) = \frac{k_{p1}A_1}{S + k_{p1}.m_{p1}.A_1}\Delta V_{01}(S) + \frac{SB_1 - k_{p1}A_1}{S + k_{p1}.m_{p1}.A_1}\Delta V_{PCC}(S) \tag{18}$$

From (18), λ can be calculated as:

$$\lambda = -k_{p1}.m_{p1}.A_1$$

The transfer function (18) has shown that the constant of the loops control can be adjusted by k_{p1}, and not by m_{p1}. The real power sharing no longer affects the quality of the voltage or frequency.

From (18), λ can be calculated as:

$$\lambda = -k_{p1}.m_{p1}.A_1$$

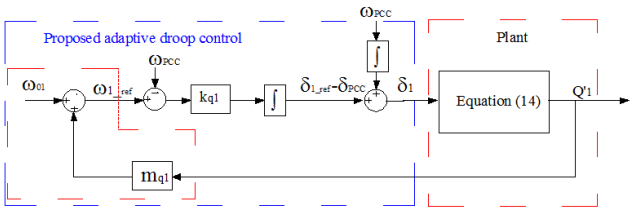

Fig. 5. Proposed adaptive reactive power sharing droop control.

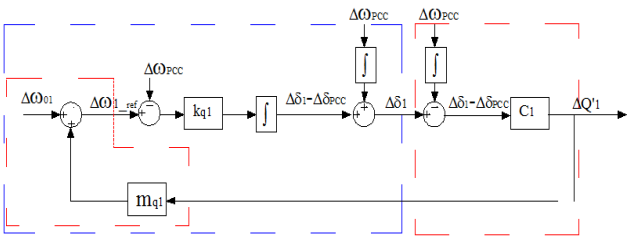

Fig. 6. Small signal adaptive reactive power sharing droop control.

2) The Proposed Reactive Power Sharing Controller

The proposed droop controller still uses equation (5) while the voltage angle of the inverter is calculated as:

$$\delta_1 = \int \omega_{PCC}\, dt + k_{q1} \int \left(\omega_{1\_ref} - \omega_{PCC}\right) dt \tag{19}$$

$$\omega_{1\_ref} = \omega_{01} + m_{q1} Q_1' \tag{20}$$

where k_{p1} is the gain of the integral and ω_{pcc} is the angular frequency at the PCC.

The relationship among (19), (20) and (14) is shown in Fig. 5.

Linearizing (14), (19) and (20) around Q_1', V_{1s}, V_{pcc}, δ_1 and δ_{pcc}, yields:

$$\Delta\omega_1 = \Delta\omega_{01} + m_{q1}\Delta Q_1' \tag{21}$$

$$\Delta\delta_1 = \Delta\delta_{PCC} + \frac{k_{q1}}{S}(\Delta\delta_1 - \Delta\delta_{PCC}) \tag{22}$$

$$\Delta Q_1' = C_1(\Delta\delta_1 - \Delta\delta_{PCC}) \tag{23}$$

where:

$$C_1 = -\frac{1}{Z_1} V_{S1} V_{PCC} \cos(\delta_1 - \delta_{PCC})$$

The relationship among (21), (22) and (23) is shown in Fig. 6.

The transfer function in Figure 6 is as follows:

$$\Delta Q_1'(S) = \frac{k_{q1} C_1}{S - k_{q1}.m_{q1}.C_1}\Delta\omega_{01}(S) - \frac{k_{q1} C_1}{S - k_{q1}.m_{q1}.C_1}\Delta\omega_{PCC}(S) \tag{24}$$

From (24), it is possible to calculate:

$$\lambda = k_{q1}.m_{q1}.C_1$$

The transfer function (24) has shown that the constant of the loops control can be adjusted by k_{p1}, and not by m_{q1}. The real power sharing no longer affects the quality of the voltage and frequency.

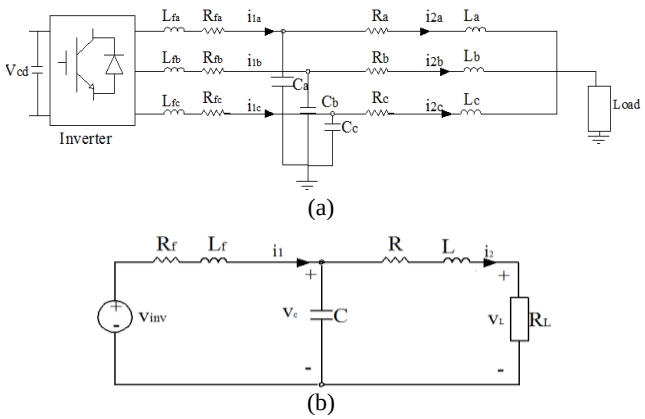

Fig. 7. (a) An equivalent three-phase circuit diagram of the inverter connected to loads; (b) an equivalent single phase circuit diagram of the inverter.

Equations (11) and (19) have shown that when the system achieves the steady-state, the measured voltage of the inverter is equal to the rated voltage. The proposed droop control solved the mismatch of power sharing caused by the different impedances of transmission lines. The controller always achieves the rated power.

B. The Line Impedance Estimation Method

1) The Recursive Least Squares Method (LSM)

An equivalent three-phase circuit diagram of the inverter connected to loads is shown in Fig. 7.

According to the equivalent circuit in Fig. 7, it is possible to write:

$$\frac{di_2}{dt} = -\frac{R}{L} i_2 + \frac{1}{L}(v_C - v_L) \tag{25}$$

Equation (25) can be rewritten as follows:

$$\begin{cases} \dot{X} = AX + Bu \\ \mathrm{Y} = \mathrm{CX} \end{cases} \tag{26}$$

where $X = i_2$, $u = v_c - v_L$, $A = -R/L$, and $B = 1/L$, $C = 1$.

By discretization of equation (26), it is possible to obtain:

$$\begin{cases} i_2(k) = A_d.i_2(k-1) + B_d.u(k-1) \\ y(k) = C_d i_2(k) \end{cases} \tag{27}$$

The transition matrix is described as follows:

$$\Phi(S) = (SI - A)^{-1} = (S + \frac{R}{L})^{-1} = \frac{1}{S + \frac{R}{L}}$$

$$\Phi(\mathrm{t}) = e^{-\frac{R}{L}t},\ A_d = \Phi(T) = e^{-\frac{R}{L}T} \approx 1 - \frac{R}{L}T$$

where T is the sample cycle used to discrete the system.

$$A_d = 1 - \frac{R}{L}T, \qquad C_d = C = 1$$

$$B_d = \int_0^T \Phi(\tau).B.d\tau = \int_0^T e^{-\frac{R}{L}\tau}.\frac{1}{L}d\tau = \frac{T}{L}$$

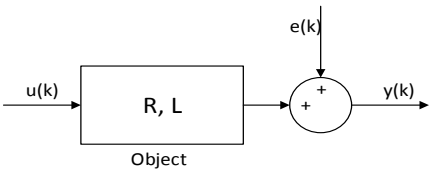

Fig. 8. Relationship between the input and output of an object.

Equation (27) represents the relationship between the input and output of the object in Fig. 8 as follows:

$$y(k) = A_d.i_2(k-1) + B_d.u(k-1) + e(k) \quad (28)$$

where *e(k)* is the measurement and process noise.

The relationship between the input and output of (28) can be written as follows:

$$y(k) = \begin{bmatrix} i_2(k-1) \\ u(k-1) \end{bmatrix}^T \begin{bmatrix} A_d \\ B_d \end{bmatrix} = \varphi(k)^T.\theta + e(k) \quad (29)$$

where *φ(k)* is the regression vector containing the variables and sample data of the voltage and current.

$$\theta = \begin{bmatrix} A_d \\ B_d \end{bmatrix} = \begin{bmatrix} 1 - \frac{R}{L}T \\ \frac{T}{L} \end{bmatrix} = \begin{bmatrix} \theta_1 \\ \theta_2 \end{bmatrix} \quad (30)$$

The problem is to estimate the parameters of vector θ based on the current data and voltage. Neglecting the noise *e(k)*, the linear regression can be predicted by:

$$\hat{y}(k,\theta) = \varphi(k)^T.\theta$$

Storing of all of the sample data in real time and calculating the volume do not increase the time a lot due to using the recursive least squares method. This algorithm includes the following equation:

$$\begin{cases} \hat{\theta}(k) = \hat{\theta}(k-1) + L(k).\varepsilon(k) \\ \varepsilon(k) = y(k) - \varphi(k)^T.\hat{\theta}(k-1) \\ L(k) = \dfrac{P(k-1)\varphi(k)}{\lambda + \varphi(k)^T.P(k-1).\varphi(k)} \\ P(k) = \dfrac{1}{\lambda}[P(k-1) - \dfrac{P(k-1).\varphi(k).\varphi(k)^T.P(k-1)}{\lambda + \varphi(k)^T.P(k-1).\varphi(k)}] \end{cases} \quad (31)$$

where λ is the forget coefficient selected in the range from 0.98 to 0.995.

The line impedance is estimated by a technique based on the recursive least squares method (LSM). The parameter vector θ_{LMS}, determined from the measured chain value, should be affected by the noise or error in equation (31). Therefore, a Kalman filter is used to filter out the noise and to obtain the approximate value of θ_{Kalman} with a real value.

2) Kalman Filter

A Kalman filter uses the recursive method to estimate the state of a process so that the average variance of the standard deviation is minimized. This makes it possible to estimate the state in the past and present. The Kalman filter has been established based on two equations, which describe the status of discrete systems. A LSM estimator and Kalman filter are shown in Fig. 9.

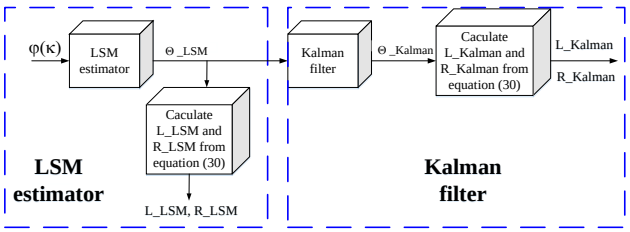

Fig. 9. LSM estimator and Kalman filter.

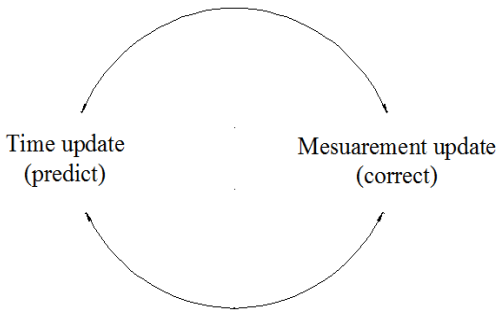

Fig. 10. Process of a Kalman filter.

The predicted state is described by the following equation:

$$x(k) = Ax(k-1) + Bu(k-1) + W_1(k) \quad (32)$$

The state measurement is described by the following equation:

$$z(k) = Hx(k) + W_2(k) \quad (33)$$

The random variables $W_{1(k)}$ and $W_{2(k)}$ are the process and measurement noise, respectively. They are assumed to be independent white noise and normal probability distributions as follows:

$$P(W_1) \sim N(0,Q) \; ; \; P(W_2) \sim N(0,R)$$

where Q is the covariance matrix of the process noise, R is the covariance matrix of the measurement noise, A is the matrix showing the relationship between state (k-1) and state k, B is the input control matrix, and H is the state matrix measurement.

3) Applying the Kalman Filter Algorithm to Filter Noise for θ

A Kalman filter is used to estimate a process by using a form of feedback control. The process of a Kalman filter is shown in Fig. 10. First, the Kalman filter estimates the state of the process at a specific time. Then, it gets feedback from the measured value to correct this estimation. Therefore, the equation of the Kalman filter is composed of two groups including the time update group and the measurement update group.

The equations for the updated time are to predict the state:

$$\begin{cases} \theta_{pred}(k) = A.\theta_{est}(k-1) & (34) \\ P_{pred}(k) = A.P_{est}(k-1).A^T + Q & (35) \end{cases}$$

The equations for the updated measurement are to correct the estimation:

$$\begin{cases} K(k) = P_{pred}(k).H^T.(H.P_{pred}(k).H^T + R)^{-1} & (36) \\ \theta_{est}(k) = \theta_{pred}(k) + K(k).\left(\theta(k) - H.\theta_{pred}(k)\right) & (37) \\ P_{est}(k) = (I - K(k).H).P_{pred}(k) & (38) \end{cases}$$

where K is the Kalman gain.

$$A = \begin{bmatrix} 1 & 0 \\ 0 & 1 \end{bmatrix}, \quad B = 0, \quad H = \begin{bmatrix} 1 & 0 \\ 0 & 1 \end{bmatrix}, \quad I = \begin{bmatrix} 1 & 0 \\ 0 & 1 \end{bmatrix}$$

The start of the Kalman filter algorithm is initialized at the initial values:

$$\theta_{est}(k-1) = \begin{bmatrix} 0 \\ 0 \end{bmatrix}, \quad P_{est}(k-1) = \begin{bmatrix} 1 & 0 \\ 0 & 1 \end{bmatrix},$$

$$Q = \begin{bmatrix} 0.001 & 0 \\ 0 & 0.001 \end{bmatrix}, R = \begin{bmatrix} 0.00025 & 0 \\ 0 & 0.00025 \end{bmatrix}$$

Equations (36)-(38) are applied to the Kalman filter and the procedure is repeated until the difference between the actual value and the value estimated is less than a predetermined error ε. The result at the output of the Kalman filter is a vector $\theta_{Kalman} = \theta_{est}$, which is determined by:

$$\theta_{Kalman} = \begin{bmatrix} \theta_{1\_Kalman} \\ \theta_{2\_Kalman} \end{bmatrix} = \begin{bmatrix} 1 - \dfrac{R_{Kalman}}{L_{Kalman}} * T \\ \dfrac{T}{L_{Kalman}} \end{bmatrix} \quad (39)$$

where T is the sample frequency, which is chosen at 5 kHz.

From (39), the values of R_{Kalman} and L_{Kalman} can be obtained.

C. The Current And Voltage Controller

The voltage and current controller employs standard proportional-integral (PI) regulators established based on the circuit equations from (40) to (43), which are written in the d_{q0} coordinates of the equivalent circuit as follows:

$$\begin{cases} i_{1d} = i_{2d} + C\dfrac{dv_{cd}}{dt} - \omega C v_{cq} & (40) \\ i_{1q} = i_{2q} + C\dfrac{dv_{cq}}{dt} + \omega C v_{cd} & (41) \end{cases}$$

$$\begin{cases} v_{inv,d} = L_f\dfrac{di_{1d}}{dt} + R_f i_{1d} - \omega L_f i_{1q} + v_{cd} & (42) \\ v_{inv,q} = L_f\dfrac{di_{1q}}{dt} + R_f i_{1q} + \omega L_f i_{1d} + v_{cq} & (43) \end{cases}$$

where i_{1d} and i_{1q} are the current amplitudes of inverter; i_{2d} and i_{2q} are the current amplitudes on the line; and v_{cd} and v_{cq} are the voltage amplitudes of the capacitor.

D. Modeling of a Single Phase SOGI-PLL

Fig. 11 shows the structure of a SOGI-PLL. Both of the adaptive filtering technique and the in-quadrature phase detection technique are used in the SOGI-PLL to generate the frequency and phase outputs. This system has a double feedback loop, i.e. the frequency/phase generator provides both the phase-angle to the Park transform and the central frequency to the second order-generalized integrator - quadrature signal generation (SOGI-QSG).

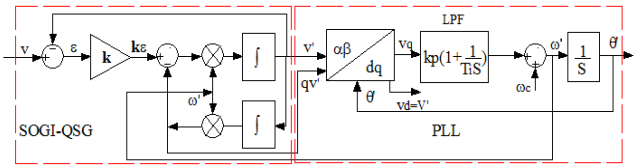

Fig. 11. Modelling of a single phase SOGI-PLL.

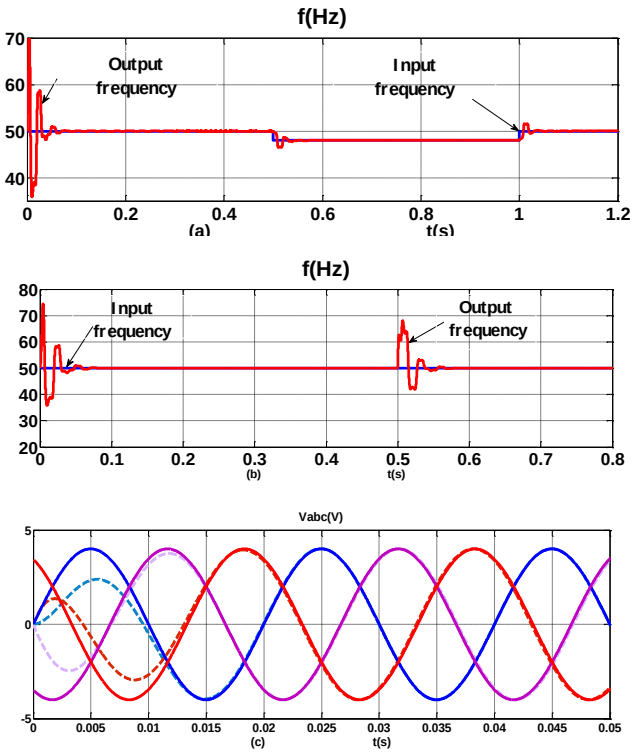

Fig. 12. Responses of a SOGI-PLL.

The parameters of the SOGI-PLL are chosen as follows: $k = \sqrt{2}$, t_s = 100ms, $\varepsilon = 1/\sqrt{2}$ and $T_i = t_s s^2/2.3 = 0.021$s. Fig. 12 shows the responses of the SOGI-PLL.

Fig. 12(a) shows the frequency response of a SOGI-PLL when the frequency of the input signal changes from 50Hz to 48Hz at t = 0.5s, and from 48Hz to 50Hz at t = 1s. Fig. 12(b) shows the frequency response of a SOGI-PLL when the phase angle of the input signal changes from 0° to 45° at t = 0.5s. Fig. 12(c) shows the response of the input and output voltages of a SOGI-PLL. The simulation results in Figure 11 show that the SOGI-PLL can obtain the exact voltage amplitude and frequency at the point of common coupling (PCC). The voltage amplitude and frequency are the input for the inner-controller. Therefore, when more exact values are obtained, more accurate power sharing is achieved.

IV. Simulation Results and Discussion

A microgrid with two parallel DG units, as shown in Fig. 1, is simulated in Matlab/Simulink. All of the simulation parameters of the system are given in Table I.

TABLE I
PARAMETERS FOR THE CONTROLLERS

Parameters	Values	Parameters	Values
Input source voltage V_{cd} (V)	600	Rate frequency f_0 (Hz)	50
Filter inductance L_f (mH)	1.2	Rate power (kVA)	5
Filter resistance R_f (Ω)	0.2	Rate voltage $V_{AC,p}$ (V)	310
Filter capacitance C (μF)	50	Droop coefficient m_q (rad/s/Var)	2.5e-4
Switching frequency f_0 (kHz)	10	Droop coefficient m_p (V/W)	1.7e-3

TABLE II
LINE PARAMETERS OF TWO INVERTERS

Line parameters	Inverter 1	Inverter 2
Resistance R (Ω)	1	1
Inductance L (mH)	5	5

TABLE III
LINE PARAMETERS OF TWO EINVERTERS

Line parameters	Inverter 1		Inverter 2	
Resistance R(Ω)	t = 0-3s	0.8	t = 0-3s	1
	t = 3-6s	0.4	t = 3-6s	0.5
	t = 6-9s	0.6	t = 6-9s	0.7
Inductance L(mH)	t = 0-3s	0.8	t = 0-3s	1
	t = 3-6s	0.4	t = 3-6s	0.5
	t = 6-9s	0.6	t = 6-9s	0.7

A. Loads Change with Fixed Line Parameters of Two Inverters

In this case, the line parameters of the two inverters are given in Table II. The simulation results for this case including the real power output, reactive power output, resistance estimation, inductance estimation, and load voltage are shown in Fig. 13.

Figs. 13(a) and 13(b) show the real and reactive power sharing of each inverter. Figs. 13(c) and 13(d) show the accuracy of the line impedance estimation method, and Figure 13€ shows the voltage quality at the PCC. Figs. 13(a) and 13(b) show that the power sharing performance is really good even when the load changes with the proposed strategy and that the voltage quality is always guaranteed. The line impedance estimation block can provide the exact resistance and inductance of the line parameters. The line resistance and inductance are estimated by the LSM method as shown in Fig. 13(c) and 13(d), respectively. However, there are some noises. Therefore, a Kalman filter is used to reduce these noises. It can be seen that the red line always has better performance than the blue line in the figures.

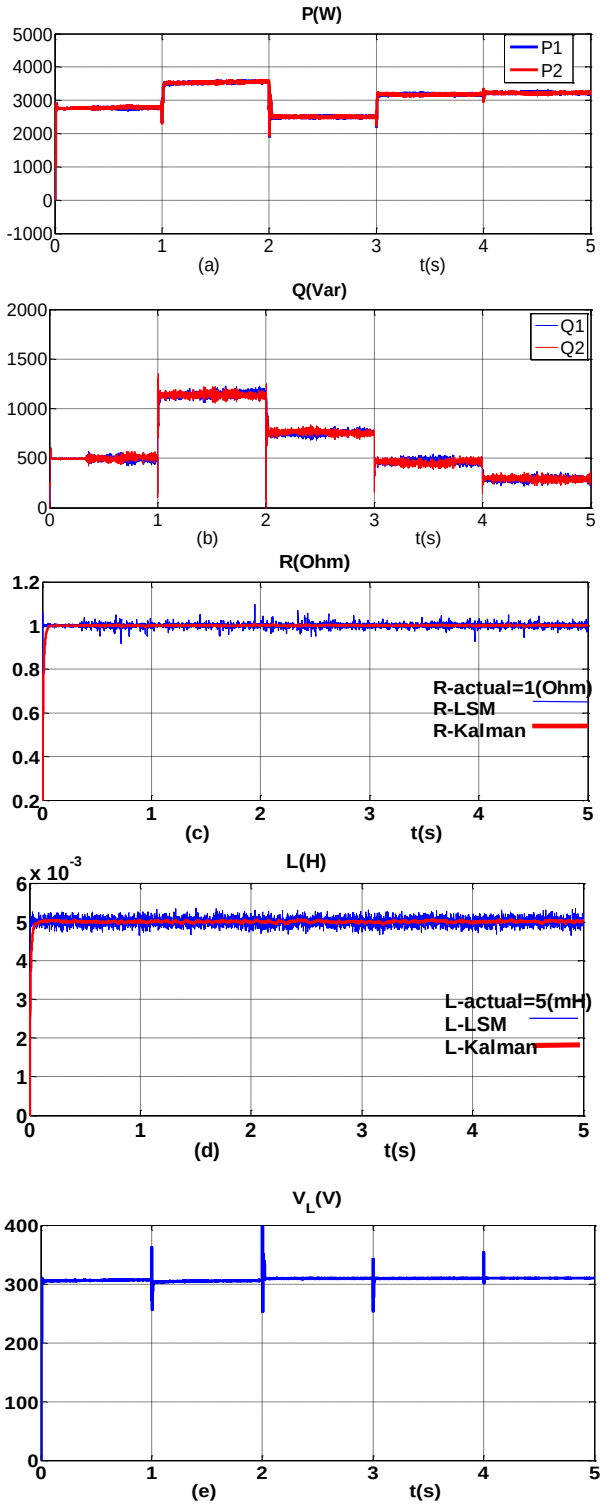

Fig. 13. (a) Real power; (b) reactive power; (c) resistance estimation; (d) inductance estimation; (e) load voltage.

B. Line Parameters Change with a Fixed Load

1) Simulation Results with the Proposed Droop Control

In this simulation, the line parameters of the two inverters are provided in Table III. The results obtained from the simulation are given in Fig. 14.

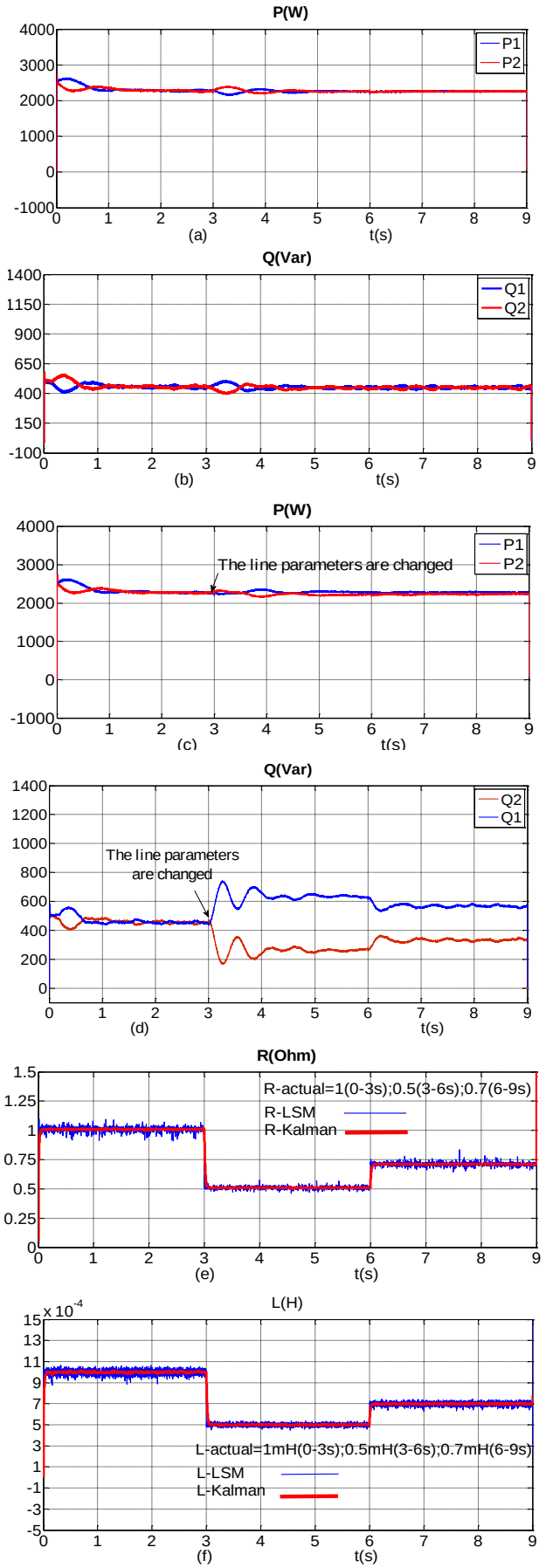

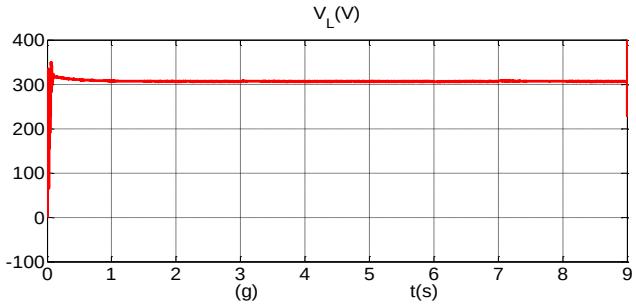

Fig. 14. (a) Real power with the line impedance estimate; (c) real power without the line impedance estimate; (b) reactive power with the line impedance estimate; (d) reactive power without the line impedance estimate; (e) resistance estimation; (f) inductance estimation; (g) load voltage.

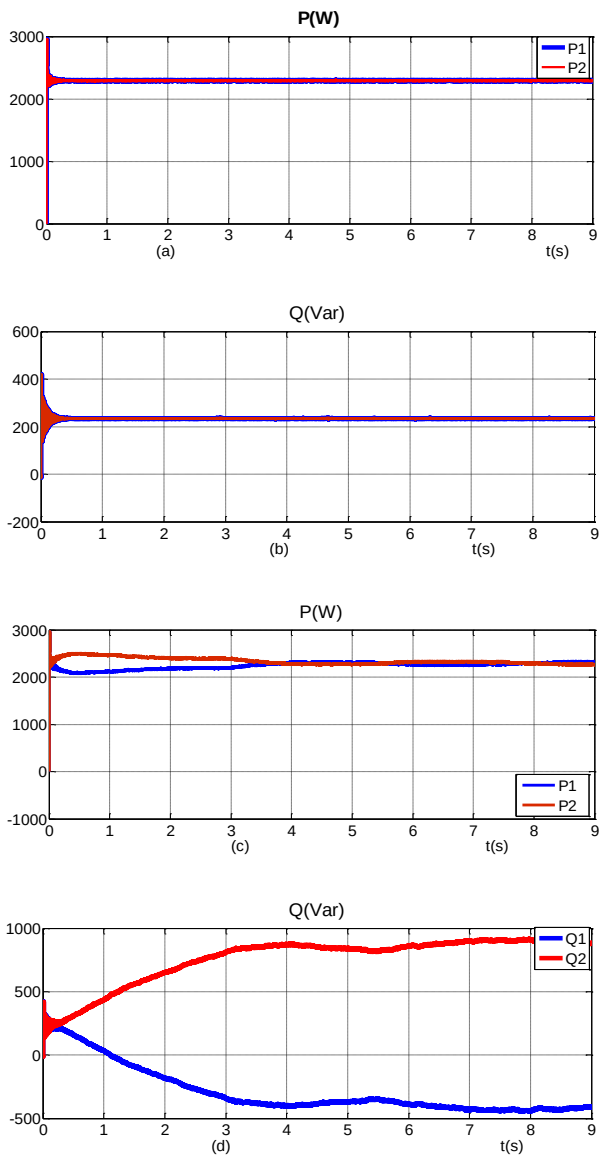

Fig. 15. (a) Active power when the line impedance does not change; (b) reactive power when the line impedance does not change; (c) active power when the line impedance changes; (d) reactive power when the line impedance changes.

TABLE IV
LINE PARAMETERS OF TWO INVERTERS

Line parameters	Inverter 1		Inverter 2	
Resistance R (Ω)	t = 0-3s	0.8	t = 0-3s	1
	t = 3-6s	0.4	t = 3-6s	0.5
	t = 6-9s	0.6	t = 6-9s	0.7
Inductance L (mH)	t = 0-3s	0.8	t = 0-3s	1
	t = 3-6s	0.4	t = 3-6s	0.5
	t = 6-9s	0.6	t = 6-9s	0.7

From Figs. 14(a) and 14(b), it can be seen that the proposed droop control method with the line impedance estimation provides a good sharing power performance for the two loads. Figs. 14(c) and 14(d) show the active power and reactive power of the two loads without using the line impedance estimation algorithm. From 0 to 3s, the line parameters are set to their real values. Therefore, the response of the sharing power of the two loads is very good. However, the real value of the line parameters changes from 3 to 9 s. It can be seen that the power sharing of the two loads cannot be implemented. Only the proposed strategy with the line impedance estimation block in Figs. 14(e) and 14(f) can share accurate real and reactive power with a 1:1 ratio. The voltage drop is always in the limit as shown Fig. 14(g).

2) Simulation Results with the Conventional Droop Control

In order to improve the performance of the reactive power sharing under the effect of the line impedance, some simulation tests have been carried out with the same scenario as in B1. However, the conventional droop control method is applied as shown in (5) and (6). The simulation results are shown in Fig. 15.

As shown in Figs. 15(a) and 15(b), the conventional method has a good performance for the case of a line impedance that is not changed. However, in the case of the line impedance changes, as shown in Table III, the active and reactive power sharing is not accurate. The line resistor does not have an effect on the reactive power sharing. However, a variation of the line resistor effects the system stability.

C. Line Parameter and Load Changes

The line parameters of the two inverters for this simulation are provided in Table IV. Simulation results are given in Fig. 15.

Figs. 16(a) and 16(b) show the high performance of the active and reactive power sharing when the proposed droop control method uses the line impedance estimation. The simulation results shown in Figs. 16(c) and 16(d) are for the case without using the line impedance estimation. It can be seen that the performance of the active and reactive power sharing is not good in the duration from 3s to 6s. Only the proposed strategy with the line impedance estimation block in Figs. 16(e) and 16(f) can share accurate real and reactive power with a 1:1 ratio.

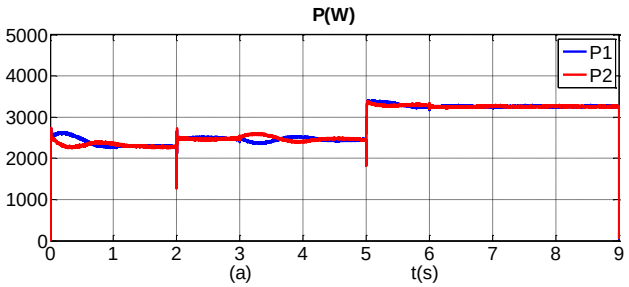

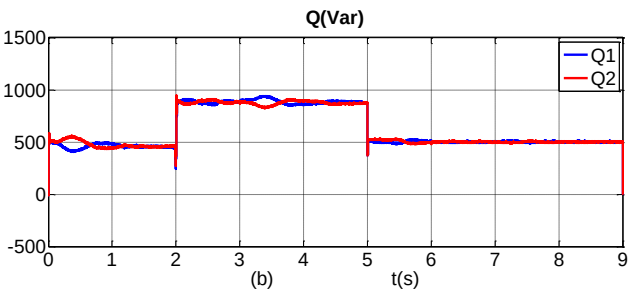

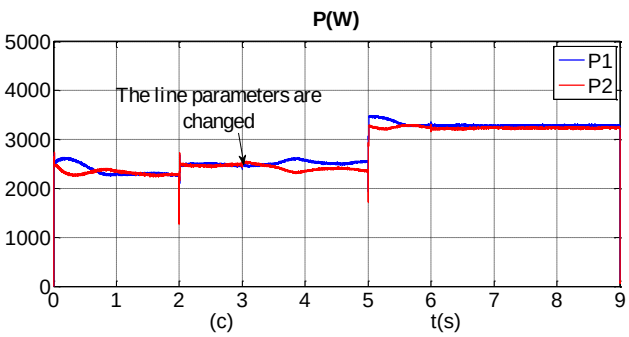

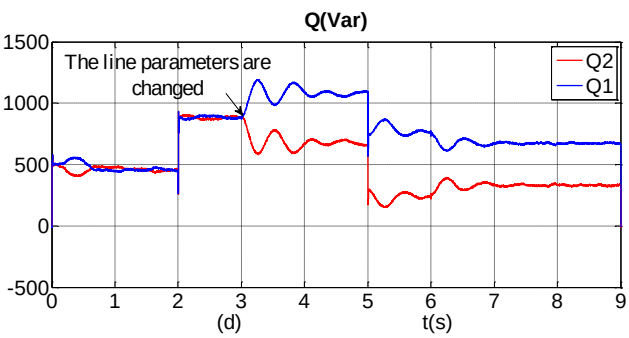

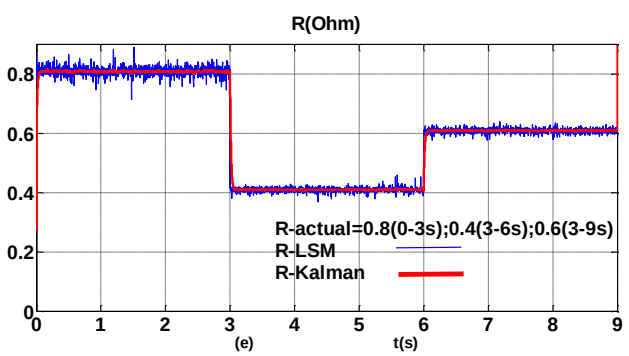

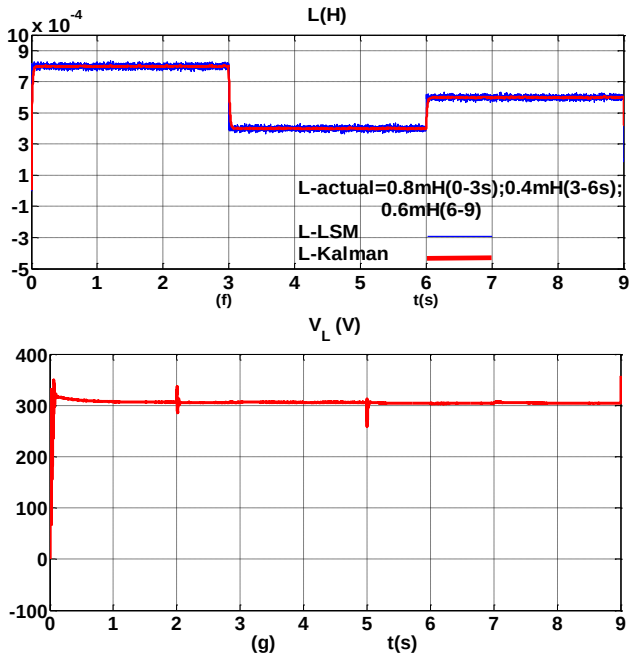

Fig. 16. (a) Real power with the line impedance estimation; (b) reactive power with the line impedance estimation; (c) real power without the line impedance estimation; (d) reactive power without the line impedance estimation; (e) resistance estimation, (f) inductance estimation; (g) load voltage.

D. Line Parameter and Load Changes

1) Simulation with the Proposed Droop Control

In this case, the rated power ratio of the inverters is 1:2, and the line parameters of the two inverters are provided in Table V. The obtained results from the simulation are given in Fig. 17.

As shown in Figs. 17(a) and 17(b), the response of the active and reactive power sharing with a ratio of 1:2 is very good even when both the load and line parameters change. Figs. 17(c) and 17(d) show simulation results of the active and reactive powers of the two loads in the case without using the line impedance estimation. From the duration 0 to 3s, the power sharing is good due to the fact that a real value is used. However, in the duration 3s-9s, if the real values of the line parameters are changed (shown in Table V), the power sharing is not good. The active and reactive powers of the two loads cannot reach the reference values.

2) Simulation with the Conventional Droop Control

Fig. 18 shows simulation results when the conventional droop control is applied with a power sharing ratio of 1:2. In the case where the three resistors are the same, the active power sharing is exactly equal to the ratio of 1:2 by the conventional method as shown in Fig. 18(a). However, the reactive power sharing is not good as shown in Fig. 18(b). In the case where the three resistors are different, as shown in Table V, power sharing with a ratio of 1:2 is not guaranteed. The conventional method cannot be applied to power sharing when the line impedances are different.

TABLE V
LINE PARAMETERS OF TWO INVERTERS

Line parameters	Inverter 1		Inverter 2	
Resistance R(Ω)	*t* = 0-3s	1	t = 0-3s	1
	t = 3-6s	0.4	t = 3-6s	0.8
	t = 6-9s	0.5	t = 6-9s	1
Inductance L(mH)	*t* = 0-3s	1	t = 0-3s	1
	t = 3-6s	0.4	t = 3-6s	0.8
	t = 6-9s	0.5	t = 6-9s	1

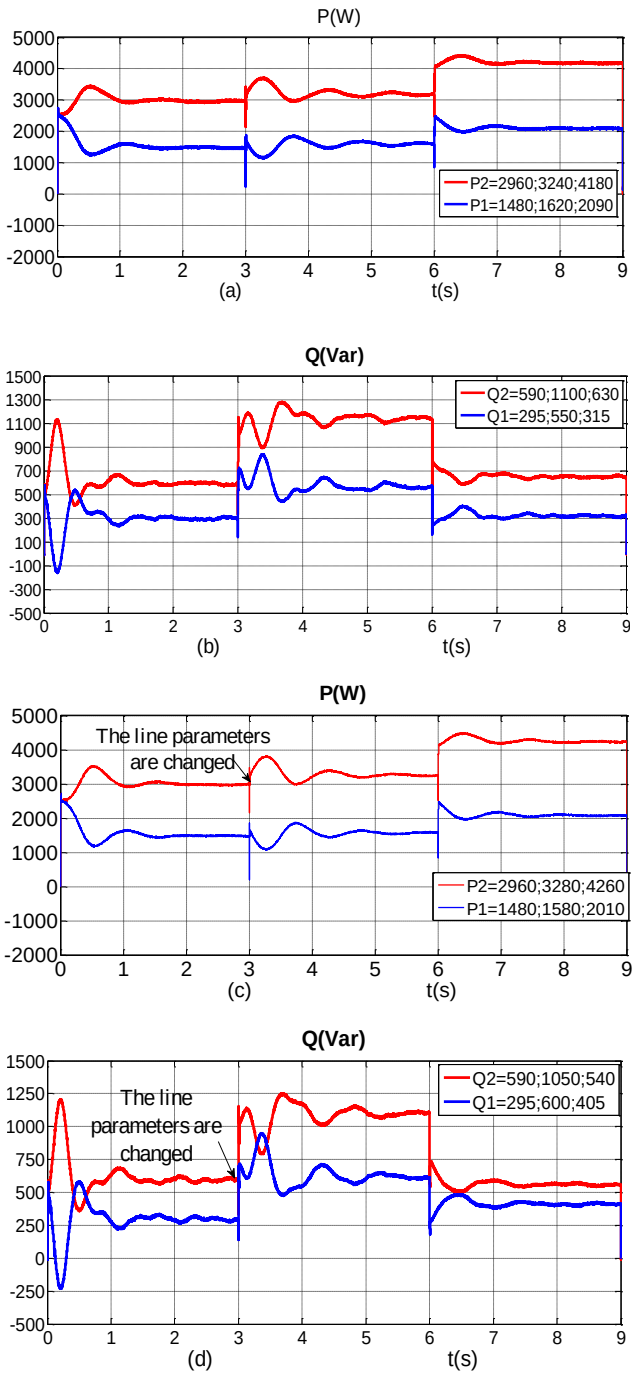

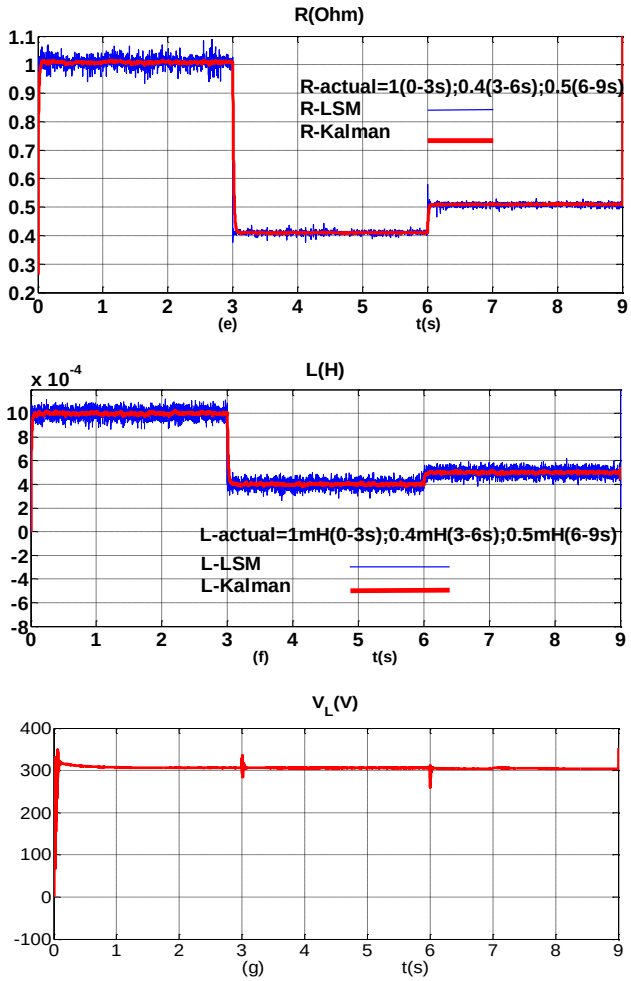

Fig. 17. (a) Real power with the line impedance estimation; (b) reactive power with the line impedance estimation; (c) real power without the line impedance estimate; (d) reactive power without the line impedance estimation; (e) resistance estimation, (f) inductance estimation; (g) load voltage.

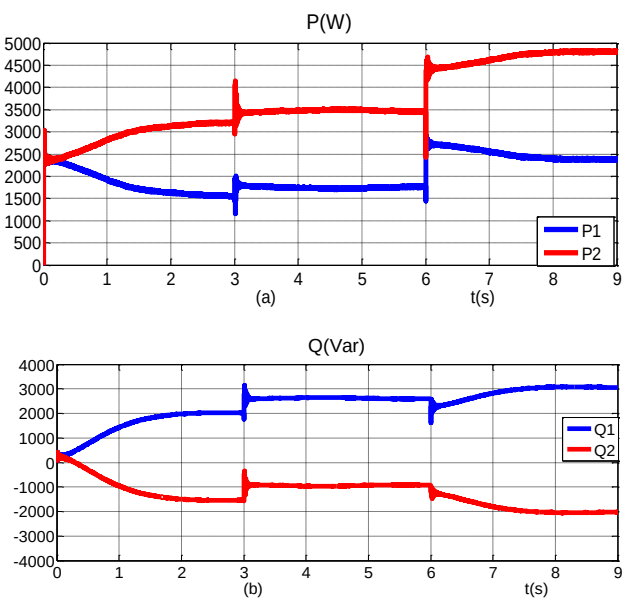

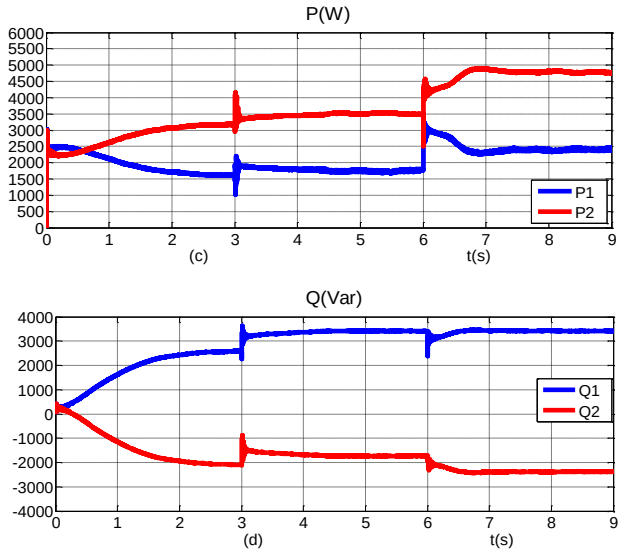

Fig. 18. (a) Active power when the three resistors are same; (b) reactive power when the three resistors are different; (c) active power when the three line resistors are the same; (d) reactive power when the three line resistors are different.

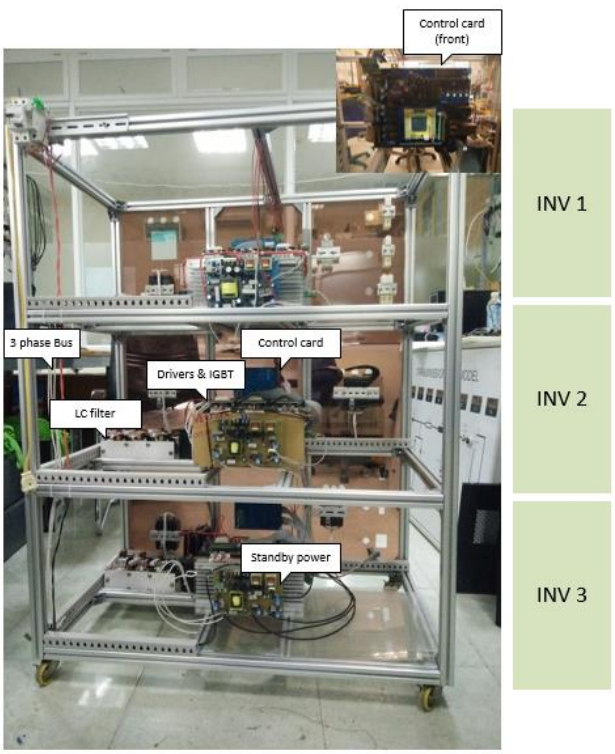

Fig. 19. Hardware setup for the experiment.

V. HARDWARE IMPLEMENTATION USING A DSP TMS320F28335

In this paper, a practical model has been developed for testing the proposed method. The developed hardware model consists of three 3-phase inverters, drivers of Semikron, LEM HX 20P and LV–25P are used as voltage and current sensors as shown in Fig. 19. The proposed control method has been

implemented on a TMS320F28335 DSP controller and the results obtained from the experiment have been captured by a Tektronix TDS2014B oscilloscope and a Fluke 345 PQ clamp meter. To maintain the load demand, the three inverters have been used with a parallel output connection while RS485 lines are used as a communication network. The experiment has been carried out on three test cases with different ratios for real and reactive powers of 1:1:1 and 1:2:3. The results obtained from the experiment have verified the advantages of the proposed control method through case studies.

A. Case Study 1: P1:P2:P3 = 1:1:1, Q1:Q2:Q3 = 1:1:1, and the Load is Fixed at a Pre-determined Value

For this case, the ratio of the active and reactive power is 1:1:1 for the three inverters with a load fixed at a pre-determined value. The measured active power outputs for the three inverters are shown in Fig. 20. The obtained active power outputs for the three inverters are P_1 = 945 W, P_2 = 935 W and P_3 = 945 W. The active power sharing errors for this case are very small.

B. Case Study 2: P1:P2:P3 = 1:1:1, Q1:Q2:Q3 = 1:1:1, and the Load Changes with Steps Within Pre-determined Limits

This case corresponds to the ratio of the active and reactive powers being 1:2:3 and load changes with steps within pre-determined limits. The measured active power outputs for the three inverters are shown in Fig. 21. The obtained active power outputs for the three inverters increase within the limits as P_{1max} = 2025 W, P_{2max} = 2045 W, P_{3max} = 2025 W, P_{1min} = 100 W, P_{2min} = 125 W and P_{3min} = 125 W. These results have demonstrated the response capability of the system based on the new control strategy when the load continuously changes online with a constant ratio.

C. Case Study 3: P1:P2:P3 = 1:2:3

The active power of the three inverters for Case study 3 with a power sharing ratio of 1:2:3 is shown in Fig. 22. The active powers of the three inverters are determined to be 865 W, 1747W and 2630 W. As observed, the active power can be shared very well.

D. Case Study 4: P1:P2:P3 = 1:1:1, Q1:Q2:Q3 = 1:1:1, and the Load Changes

Fig. 23 shows the active and reactive powers of the three inverters in case of load changes. It can be seen that the ratio of the active and reactive powers is still kept at 1:1:1 when the load increases and decreases.

E. Case Study 5: Estimating the R and L Values when the Temperature is 20oC

In this case study, the actual values of R and L are given as R_{actual} = 4.9Ω and L_{actual} = 0.0069H. Fig. 24(a) shows the

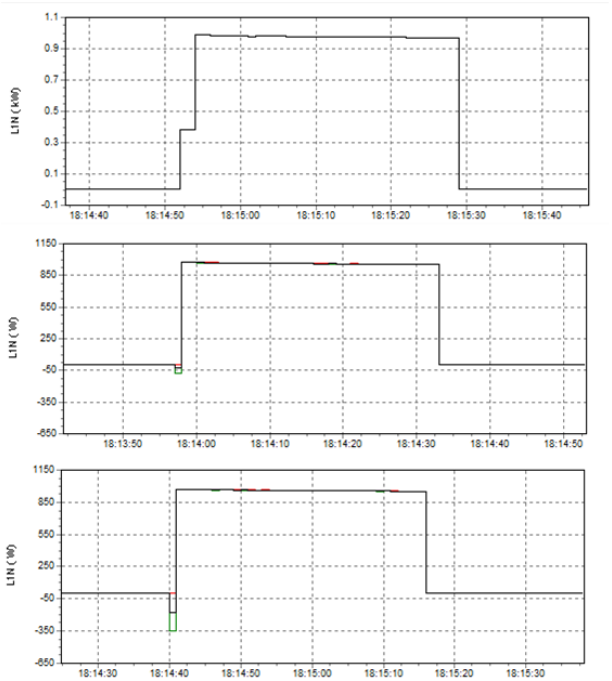

Fig. 20. Real power of the three inverters for Case study 1.

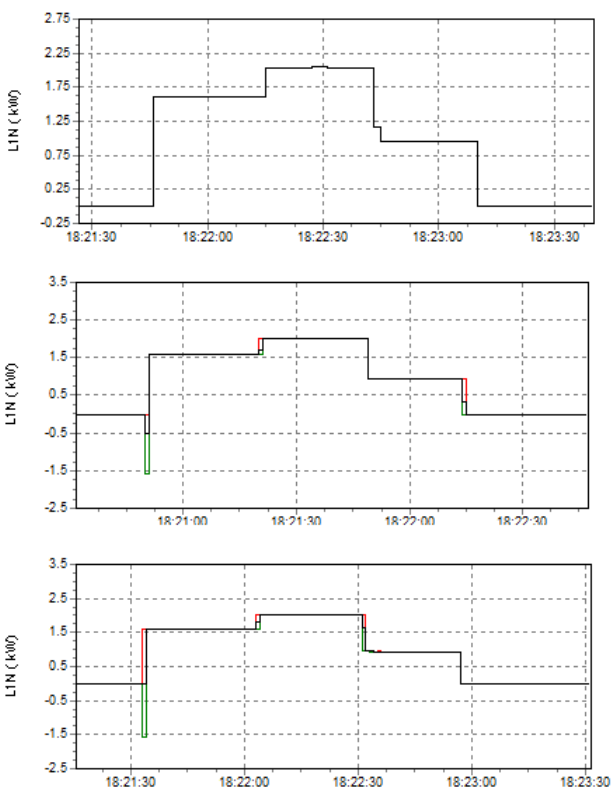

Fig. 21. Active power of the three inverters for Case study 2.

estimation of the R value by using the SLM method, where the variation of this value is from 4.88Ω to 4.935Ω. These errors are caused by the noise of the current and voltage measurements. The R value shown in Fig. 24(b) is obtained

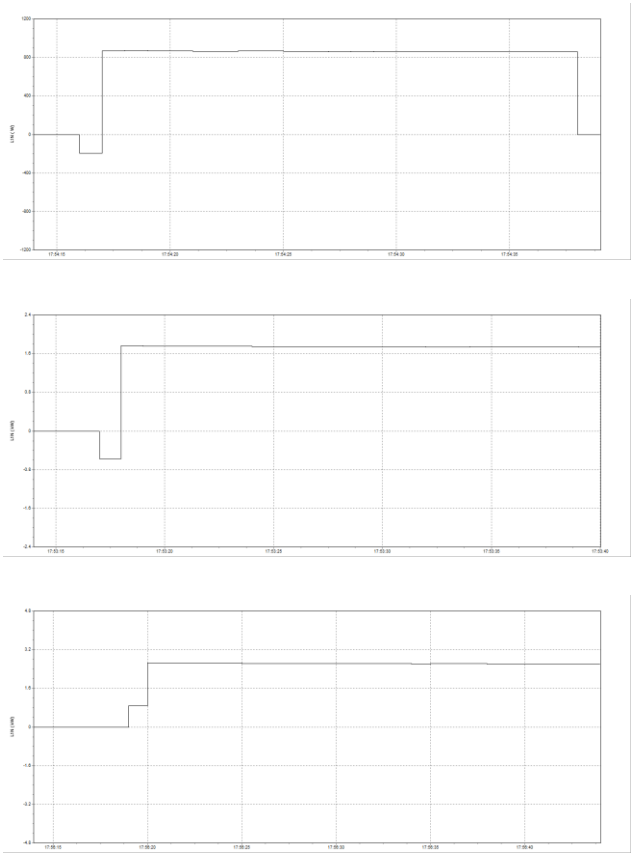

Fig. 22. Active power of the three inverters for Case study 3.

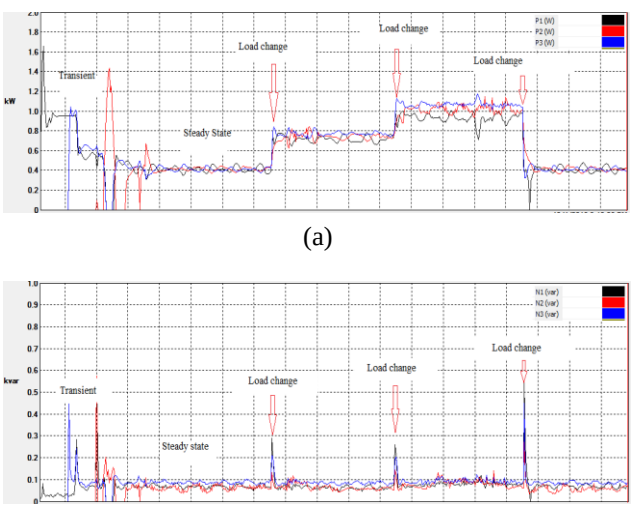

(a)

(b)

Fig. 23. Three inverters for Case study 4: (a) active power; (b) reactive power.

by applying a Kalman filter. It can be seen that the peak-to-peak variation is reduced.

Fig. 25(a) shows that the LSM method provides an accuracy value for *L*. The variation of *L* is from 0.00674H to 0.007065H. In order to reduce this variation, a Kalman filter is applied and the estimated value of *L* is shown in Fig. 25(b).

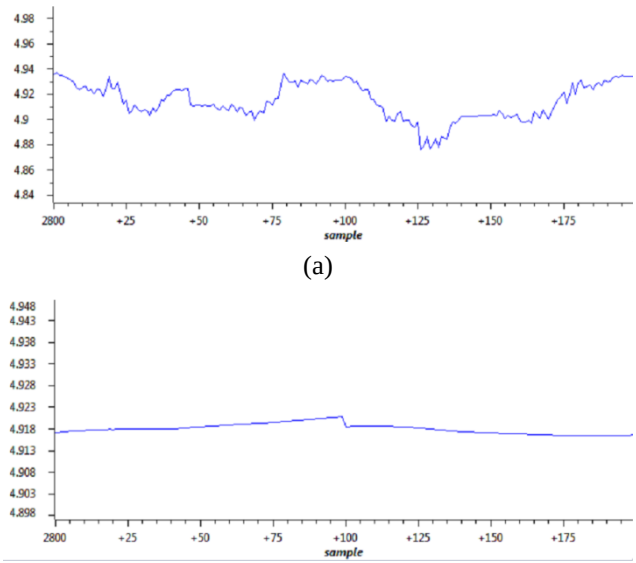

(a)

(b)

Fig. 24. Estimated value of R in the case of: (a) using the LSM method; (b) using the LSM method and applying a Kalman filter.

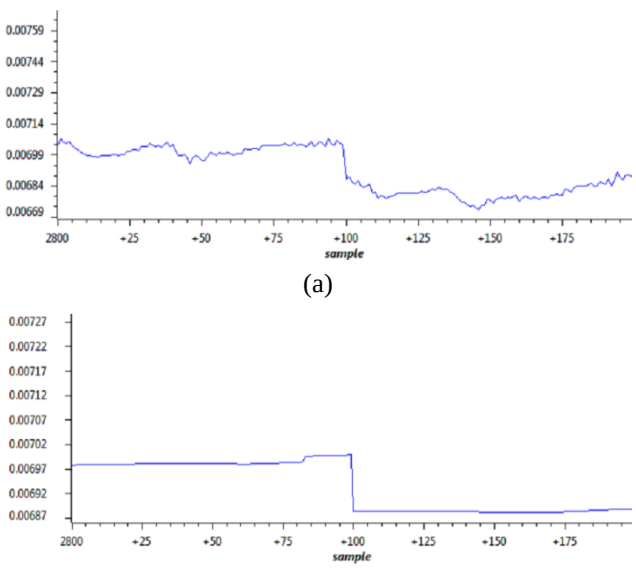

(a)

(b)

Fig. 25. Estimated value of *R* in the case of: (a) using the LSM method; (b) using the LSM method and applying a Kalman filter.

F. Case Study 6: Estimating the R Value When the Temperature is 42^0C

The experiment is repeated for the temperature increasing to 42^0C. The actual value of *R* is 5.5Ω. By using the proposed method, the estimated value of *R* is shown in Figs. 26(a) and 26(b) in case of using the LSM method and the LSM method with a Kalman filter, respectively. It can be seen that the proposed method can provide a good estimation for *R* and *L*. These experimental results have verified the theoretical analysis.

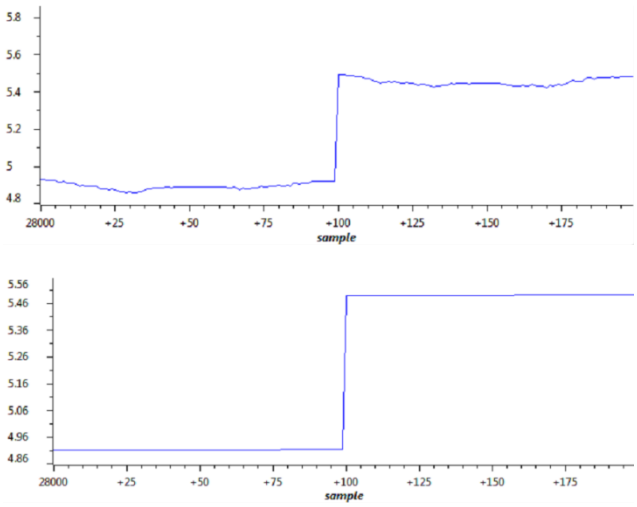

Fig. 26. Estimated value of *R* in the case of: (a) using the LSM method; (b) using the LSM method and applying a Kalman filter.

VI. Conclusion

This paper has proposed a new method of droop control for an accurate load sharing ratio between the paralleled inverters in islanded microgrids with the line impedance estimated online in terms of the conventional resistor. In this study, the line impedance may vary due to changes in temperature or frequency at the same time as significant differences between the inverters. The estimation blocks provide the line impedance parameters in real-time for the proposed droop controller, which was built based on the minimum squares algorithm combined with a Kalman filter. Even though the line impedances and load change at the same time, the refresh rate is fast enough to keep the system stabile with a high accuracy power sharing. Simulation results in Matlab/ Simulink and hardware experiments have demonstrated the superiority of the proposed strategy in any case with any ratio.

Acknowledgement

The authors would like to acknowledge the support from the Power Electronics Research of HCMUT. This research is funded by VNU-HCM under grant number B2016-20-07.

References

[1] H. Han, X. Hou, J. Yang, J. Wu, M. Su, and J. M. Guerrero, "Review of power sharing control strategies for islanding operation of AC microgrids," *IEEE Trans. Smart Grid*, Vol. 7, No. 1, pp. 200-216, Jan. 2016.

[2] K. Moslehi and R. Kumar, "A reliability perspective of the smart grid," *IEEE Trans. Smart Grid*, Vol. 1**,** No. 1, pp. 57-64, Jan. 2010.

[3] R. H. Lasseter, "Microgrids," *in Proc. IEEE Power Eng. Soc. Winter Meeting*, pp. 305-308, 2002.

[4] R. H. Lasseter and P. Paigi, "Microgrid: A conceptual solution," in *Proc. IEEE Power Electron. Spec. Conf.*, pp. 4285-4290, 2004.

[5] J. Rocabert, A. Luna, F. Blaabjerg, and P. Rodriguez, "Control of power converters in AC microgrids," *IEEE Trans. Power Electron.*, Vol. 27, No. 11, pp. 4734-4739 Nov. 2012.

[6] A. Molderink, V. Bakker, M. G. C. Bosman, J. L. Hurink, and G. J. M. Smit, "Management and control of domestic smart grid technology," *IEEE Trans. Smart Grid*, Vol. 1, No. 2, pp. 109-119, Mar. 2010.

[7] F. Blaabjerg, R. Teodorescu, M. Liserre, and A. V. Timbus, "Overview of control and grid synchronization for distributed power generation systems," *IEEE Trans. Ind. Electron.*, Vol. 53, No. 5, pp. 1398-1409, May 2006.

[8] Q.-C. Zhong, "Robust droop controller for accurate proportional load sharing among inverters operated in parallel," *IEEE Trans. Power Electron*., Vol. 60, No. 4, pp. 1281-1291, Apr. 2013.

[9] R. Lasseter, "Microgrids," in *Proc. IEEE Power Eng. Soc. Winter Meeting*, pp. 305–308, 2002.

[10] G. Weiss, Q.-C. Zhong, T. C. Green, and J. Liang, "H∞ repetitive control of DC-AC converters in microgrids," *IEEE Trans. Power Electron.*, Vol. 19, No. 1, pp. 219-230 Jan. 2004.

[11] J. Guerrero, J. Vasquez, J. Matas, M. Castilla, and L. García de Vicuña, "Control strategy for flexible microgrid based on parallel line-interactive UPS systems," *IEEE Trans. Ind. Electron.*, Vol. 56, No. 3, pp. 726-736, Mar. 2009.

[12] S. V. Iyer, M. N. Belur, and M. C. Chandorkar, "A generalized computational method to determine stability of a multi-inverter microgrid," *IEEE Trans. Power Electron.*, Vol. 25, No. 9, pp. 2420-2432, Sep. 2010.

[13] J. Justo, F. Mwasilu, and J. Lee, "AC microgrids versus DC microgrids with distributed energy resources: A review," *Renew. Sustain. Energy Rev.*, Vol. 24, pp. 387-405, 2013.

[14] M. A. Eltawil and Z. Zhao, "Grid-connected photovoltaic power systems: Technical and potential problems – A review," *Renew. Sustain. Energy Rev.*, Vol. 14, No. 1, pp. 112-129, 2010.

[15] J. Guerrero, L. García de Vicuña, J. Matas, M. Castilla, and J. Miret, "Output impedance design of parallel-connected UPS inverters with wireless load-sharing control," *IEEE Trans. Ind. Electron.*, Vol. 52, No. 4, pp. 1126-1135, Apr. 2005.

[16] P. Piagi and R. H. Lasseter, "Autonomous control of microgrids," in Proc. Power Eng. Soc. Gen. Meeting (2006), pp. 8-15.

[17] M. C. Chandorkar, D. M. Divan, and R. Adapa, "Control of parallel connected inverters in standalone AC supply systems," *IEEE Trans. Ind. Appl.*, Vol. 29, No. 1, pp. 136-143, 1993.

[18] J. M. Guerrero, J. C. Vasquez, and J. Matas, "Control strategy for flexible microgrid based on parallel line-interactive UPS systems," *IEEE Trans. Ind. Electron.*, Vol. 56, No. 3, pp. 726-736, Mar. 2009.

[19] J. Hu, J. Zhu, D. G. Dorrell, and J. M. Guerrero, "Virtual flux droop method - A new control strategy of inverters in microgrids," *IEEE Trans. Power Electron.*, Vol. 29, No. 9, pp. 4704-4711, Sept. 2014.

[20] L. Y. Lu and C. C. Chu, "Consensus-based droop control synthesis for multiple DICs in isolated micro-grids," *IEEE Trans. Power Syst.*, Vol. 30, No. 5, pp. 2243-2256, Sept. 2015.

[21] J. He and Y. W. Li, "An enhanced microgrid load demand sharing strategy," *IEEE Trans. Power Electron.*, Vol. 27, No. 9, pp. 3984-3995, Sep. 2012.
[22] W. Yao, M. Chen, and J. Matas, "Design and analysis of the droop control method for parallel inverters considering the impact of the complex impedance on the power sharing," *IEEE Trans. Ind. Electron.*, Vol. 58, No. 2, pp. 576-588, Feb. 2011.
[23] Hisham Mahmood, Dennis Michaelson, and Jin Jiang "Accurate reactive power sharing in an islanded microgrid using adaptive virtual impedances," *IEEE Trans. Power Electron.*, Vol. 30, No. 3, pp. 1605-1618 Mar. 2015.
[24] J. M. Guerrero, M. Chandorkar, T.-L. Lee, and P. C. Loh, "Advanced control architecture for intelligent microgrids - Part I: Decentralized and hierarchical control," *IEEE Trans. Power Electron.*, Vol. 60, No. 4, pp. 1254-1262 Apr. 2013.
[25] J. M. Guerrero, J. C. Vasquez, J. Matas, L. G. de Vicuna, and M. Castilla, "Hierarchical control of droop-controlled ac and dc microgrids - A general approach towards standardization," *IEEE Trans. Ind. Electron.*, Vol. 58, No. 1, pp. 158-172, Jan. 2011.
[26] M. N. Marwali, J.-W. Jung, and A. Keyhani, "Control of distributed generation systems – Part II: Load sharing control," *IEEE Trans. Power Electron.*, Vol. 19, No. 6, pp. 1551-1561, Jun. 2004.
[27] J. C. Vasquez, J. M. Guerrero, M. Savaghebi, J. Eloy-Garcia, and R. Teodorescu, "Modeling, analysis, and design of stationary-reference frame droop-controlled parallel three-phase voltage source inverters," *IEEE Trans. Ind. Electron.*, Vol. 60, No. 4, pp. 1271-1280, Apr. 2013.
[28] M. Savaghebi, A. Jalilian, J. C. Vasquez, and J. M. Guerrero, "Secondary control scheme for voltage unbalanced compensation in an islanded droop controlled microgrid," *IEEE Trans. Smart Grid*, Vol. 3, No. 2, pp. 797-807, May 2012.
[29] M Savaghebi, A. Jalilian, J. C. Vasquez, and J. M. Guerrero, "Secondary control for voltage quality enhancement in microgrids," *IEEE Trans. Smart Grid*, Vol. 3, No. 4, pp. 1893-1902, May 2012.
[30] M. A. Abusara, J. M. Guerrero, and S. M. Sharkh, "Line-interactive ups for microgrids," *IEEE Trans. Ind. Electron.*, Vol. 61, No. 3, pp. 1292-1300, Mar. 2014.
[31] Juan C. Vasquez, Josep M. Guerrero, Alvaro Luna, Pedro Rodríguez, and Remus Teodorescu "Adaptive droop control applied to voltage-source inverters operating in grid-connected and islanded modes," *IEEE Trans. Ind. Electron.*, Vol. 56, No. 10, pp. 4088-4098, Oct. 2009.
[32] D. De and V. Ramanarayanan, "Decentralized parallel operation of inverters sharing unbalanced and nonlinear loads," *IEEE Trans. Power Electron.*, Vol. 25, No. 12, pp. 3015-3025, Dec. 2010.
[33] Y. W. Li and C.-N. Kao, "An accurate power control strategy for power-electronics-interfaced distributed generation units operating in a low-voltage multibus microgrid," *IEEE Trans. Power Electron.*, Vol. 24, No. 12, pp. 2977-2988, Dec. 2009.
[34] H. Mahmood, D. Michaelson, and J. Jiang, "Accurate reactive power sharing in an islanded microgrid using adaptive virtual impedances," *IEEE Trans. Power Electron.*, Vol. 30, No. 3, pp. 1605-1617, Mar. 2014.
[35] J. He, Y. W. Li, J. M. Guerrero, J. C. Vasquez, and F. Blaabjerg, "An islanded microgrid reactive power sharing scheme enhanced by programmed virtual impedances," *in Proc. IEEE Int. Symp. Power Electron. Distrib. Gener. Syst.* 2012, pp. 229-235.
[36] J. He, Y. W. Li, J. M. Guerrero, F. Blaabjerg, and J. C. Vasquez, "An islanding microgrid power sharing approach using enhanced virtual impedance control scheme," *IEEE Trans. Power Electron.*, Vol. 28, No. 11, pp. 5272-5282, Nov. 2013.

Phuong Minh Le was born in Vietnam, in 1973. He received M.S. degree in Electrical Engineering from Kharkov State Academy, Kharkov, Ukraine, in 1997; and the Ph.D. degree from the Department of Automated Electromechanical Systems, Kharkov National Technical University, Kharkov, Ukraine, in 2001. He is currently working as a Lecturer in the Faculty of Electrical and Electronics Engineering, Ho Chi Minh City University of Technology, Ho Chi Minh City, Vietnam. His current research interests include power converters in microgrids, renewable energy, power electronics, power converters, and motor drives.

Xuan Hoa Thi Pham received the M.S. degree from the Hochiminh City University of Technology, Ho Chi Minh City, Vietnam, in 2006. She has been a Lecturer of Department of Electrical and Electronic Engineering at the University of Food Industry, Ho Chi Minh City, Vietnam, since 2002. Her current research interests include renewable energy interfaces, microgrids and power quality.

Huy Minh Nguyen was born in Dong Thap, Vietnam, in 1989. He received his B.S. and M.S. degrees in Automatic Control Engineering from the Ho Chi Minh City University of Technology, Ho Chi Minh City, Vietnam, in 2012 and 2014, respectively. He is presently working towards his Ph.D. degree at École de Technologie Supérieure, Montreal, QC, Canada. His current research interests include DC/DC converters and renewable energy.

Duc Duy Vo Hoang was born in Vietnam, in 1991. He received his B.S. degree in Electrical Engineering from the Ho Chi Minh City University of Technology, Ho Chi Minh City, Vietnam, in 2016, where he is presently working toward his M.S. degree in Electrical Engineering. His current research interests include power converters in microgrids and renewable energy.

Tuyen Dinh Nguyen (M'13) was born in Binh Dinh, Vietnam, in 1982. He received the B.S. degree in electrical engineering from Ho Chi Minh City University of Technology, Vietnam, in 2004, and the Ph.D. degree from the University of Ulsan, Ulsan, Korea in 2012. He is currently working as a Lecturer in the Faculty of Electrical and Electronics Engineering, Ho Chi Minh City University of Technology. His current research interests include power electronics, electrical machine drives, low-cost inverters, renewable energy, matrix converters and microgrids.

Dieu Ngoc Vo received his B.Eng. and M.Eng. degrees in electrical engineering from Ho Chi Minh City University of Technology, Ho Chi Minh city, Vietnam, in 1995 and 2000, respectively and his D.Eng. degree in energy from Asian Institute of Technology (AIT), Pathumthani, Thailand in 2007. He is Research Associate at Energy Field of Study, AIT and Head of Department of Power Systems, Faculty of Electrical and Electronic Engineering, Ho Chi Minh City University of Technology, Ho Chi Minh city, Vietnam. His research interests are applications of AI in power system optimization, power system operation and control, power system analysis, and power systems under deregulation and restructuring.